Interfacial conditions during evaporation or condensation of water

C. A. Ward* and D. Stanga
Thermodynamics and Kinetics Laboratory, Department of Mechanical Engineering and Industrial Engineering, University of Toronto, 5 King's College Road, Toronto, Canada M5S 3G8

(Received 16 April 2001; revised manuscript received 15 June 2001; published 29 October 2001)

Steady-state evaporation and condensation experiments have been conducted with water under conditions where buoyancy-driven convection is not present. The temperature profile in each phase has been measured. At the interface, independently of the direction of the phase change, a temperature discontinuity has been found to exist in which the interfacial vapor temperature is greater than that in the liquid. In a thin layer immediately below the interface the temperature is uniform in a layer ($\sim$0.5 mm) and below that the temperature profile is linear, indicating thermal conduction. The uniform temperature layer indicates a mixing process occurs near the interface that could result from surface-tension driven (Marangoni-Bénard) convection and/or from ''energy partitioning'' that is necessary to account for the measured temperature discontinuity near the interface. When the measured interfacial properties are used with the expression for the phase change rate that is obtained from statistical rate theory, it is found that the predictions are in close agreement with the measurements.

DOI: 10.1103/PhysRevE.64.051509 PACS number(s): 64.70.Fx

I. INTRODUCTION

The conditions existing at the liquid-vapor interface during a phase change process are not well understood, possibly because of uncertainties in the thermodynamic conditions at the interface and/or the possible presence of convection. Classical kinetic theory has provided the molecular basis for the understanding of evaporation for over a century [1–4]. Initial progress with mercury showed promise, but with other liquids and particularly water, the results were less certain. Although classical kinetic theory does not lead to a prediction of the liquid-vapor phase change rate, it has been used to define two empirical parameters, the evaporation and condensation coefficients, β_e and β_c [3], and these coefficients have been used to correlate a large number of measurements. Marek and Straub [5] have recently surveyed the reported values of these coefficients for water and pointed out the wide variation at nominally the same experimental conditions. The results of this survey suggest that the basic definitions of these coefficients is inadequate in some as yet undefined way, or that the experiments are not being performed under the conditions assumed.

One of the possible experimental difficulties is convection—either buoyancy or surface-tension driven. Although surface-tension driven (or Marangoni-Bénard) convection has been well documented for fluids other than water [6,7], Cammenga *et al.* [8] have pointed out the absence of experimental evidence for water. This absence is often attributed to contamination. However, in the experiments of Barnes and Hunter [9] and particularly those of Cammenga, Schreiber and Rudolph [10] and Schreiber and Cammenga [11] measures were taken to ensure cleanliness, but none of these studies indicated the presence of Marangoni-Bénard convection [8].

However, one of the difficulties is knowing whether convection should be expected. In the analytical investigations to determine the criterion, it is usually assumed that the liquid phase is a continuum with no phase change at the free (liquid-vapor) surface—only cooling or heating [12–14]. This leaves out the flow field required to supply (or remove) liquid to the interface where the evaporation (or condensation) is taking place. Further, experimental observations do not appear to support the criterion developed from these analytical approaches. Using an experimental approach in which several liquids, but not water, were studied, Chai and Zhang found that the traditional criterion for the onset of Marangoni-Bénard convection was not in agreement with their observations, and they suggested a modified criterion [6]. If the analytical criterion for the onset of surface-tension driven convection is to be improved, it seems necessary to know the coupling between the local-equilibrium properties at the liquid-vapor interface and the evaporation or condensation flux. This coupling relation is unlikely to be predicted from a continuum formulation or classical kinetic theory [5].

An expression for the evaporative flux that shows promise of providing this relation has been obtained from statistical rate theory (SRT) [15–20]. This approach uses the transition probability concept of quantum mechanics, assumes the quantum-mechanical states within the energy uncertainty of an isolated system are equally probable, and that the rate of exchange between these quantum states has the same value. It leads to an expression for the phase change rate that depends only on the material and molecular properties of the fluid undergoing the phase change process and on the local-equilibrium properties at the interface in each phase (see the Appendix). For water, the material and molecular properties are known.

The expression obtained from statistical rate theory for the phase change rate has been previously examined for evaporation, and the predictions were found to be in close agreement with the measurements for three different liquids

*Corresponding author. Present address: Dept. of Mechanical Engineering and Industrial Engineering, 5 King's College Road, Toronto, Canada M5S 3G8. FAX: 416-978-7322. Email address: ward@mie.utoronto.ca

[21–23]. Theoretically the same expression should be valid when the net molecular flux is reversed, i.e., for condensation (negative evaporation), but it has not been previously examined for condensation. For this purpose, a coordinated series of steady-state evaporation and condensation experiments have been conducted. Since water expands on cooling for temperatures less than 4 °C, experiments were conducted under conditions where no buoyancy-driven convection during either evaporation or condensation would be present. The temperature profile was measured in both phases near the interface using small (~25 μ diameter) thermocouples. The profile indicates that independently of the direction of the net molecular transport, the interfacial vapor temperature is higher than that in the liquid, that there is a thin layer of liquid (~0.5-mm deep) near the interface in which the temperature is uniform, and that below the uniform temperature layer, the mode of energy transport is by conduction. Using the measured interfacial temperatures, flux rate and interface curvature, the SRT expression for the phase change rate may be used to predict the pressure in the vapor and the results compared with the measurements.

The analysis raises a kinetics issue. In classical kinetic theory, the unidirectional liquid evaporation rate is usually assumed to be independent of the conditions in the vapor phase [1–4], whereas, the SRT expression for the phase change rate depends on the entropy change that results from one molecule transferring from the liquid to the vapor phase, Δs_{LV} and this quantity depends on the conditions in both phases. This predicted dependence of the SRT phase change rate is evaluated by comparing the measurements with the predictions.

II. EXPERIMENTAL METHODS

Water was deionized, distilled, nanofiltered, degassed, and held in a sealed glass vessel that was connected to a syringe pump through a valve. As indicated in Fig. 1, a second outlet from the syringe led to a conical funnel (7-mm-mouth diameter) in the phase-change chamber through a 1.5-mm-diam stainless-steel tube. Before water was transferred to the syringe, the chamber and syringe were evacuated to a pressure of less than 10^{-3} Pa with a vacuum system. Afterwards the valve between the syringe and the glass container was opened and water was allowed to flow from the glass container into the syringe. The syringe pump pushed water to the funnel mouth where a liquid-vapor interface was formed.

The chamber was then pressurized with N_2 to 0.4 MPa for 1 h to force water into any cavities that may have been left unfilled when the test liquid was introduced. Afterwards the chamber was decompressed to near atmospheric and half of the water in the syringe pump was expelled through the funnel and drained from the chamber. Ideally, this removed the water containing dissolved N_2. Finally, the chamber was evacuated for 1 h to dry the chamber. Degassed water remained in the syringe and funnel. The syringe pump was then advanced until the water-vapor interface was again at the mouth of the funnel. The system was ready to run an evaporation experiment. To run a condensation experiment, one additional preparation step was required.

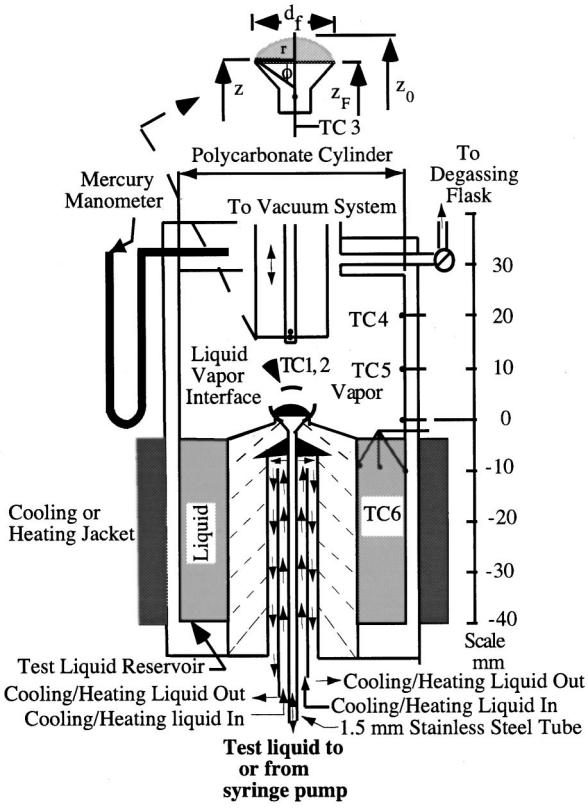

FIG. 1. Schematic of the phase-change chamber and definition of the interface shape parameters, d_f and $(z_0 - z_F)$.

When an evaporation experiment was to be performed, a valve between the chamber and the vacuum system was opened slightly, initiating evaporation. From outside the chamber, the height of the water-vapor interface could be measured with a cathetometer to ± 10 μm. Both the syringe pumping rate and the valve to the vacuum system were adjusted until the liquid-vapor interface remained at a constant height. The steady-state evaporation rate was then equal to the pumping rate. The latter could be measured to ± 0.3 μL (liquid)/h.

When a condensation experiment was to be run, the same procedure was followed to establish a water-vapor interface at the mouth of the funnel. Afterwards, prepared water was allowed to flow, without exposure to air, into the concentric test liquid reservoir indicated in Fig. 1. A heating jacket maintained the reservoir-water temperature at a predetermined value. The water in the funnel was then cooled by flowing a cooling fluid into the tube that was concentric to the tube leading from the syringe to the funnel (see Fig. 1). This caused vapor coming from the test-liquid reservoir in the chamber to condense at the liquid-vapor interface that was maintained at the funnel mouth. The reversible syringe pump was then used to withdraw water from the funnel at a rate that maintained the interface at a constant height. In this circumstance, the steady-state condensation rate was equal to the withdrawal rate of the syringe pump, and could be measured with the same accuracy as the evaporation rate. Thus, during either an evaporation or a condensation experiment,

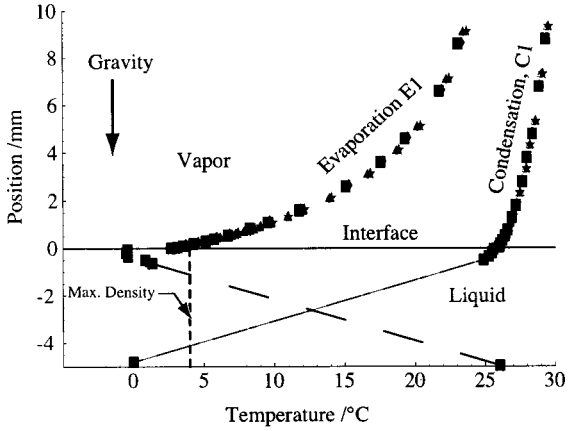

FIG. 2. Measured temperature profiles on the phase-change chamber center line during steady-state evaporation or condensation (experiments E1 and C1, see Table I). During each experiment, two temperature profiles were measured at least 30 min apart. The temperature profile in the liquid phase of C1 is an approximate inversion of the temperature profile in the liquid phase during E1. Note the agreement between the differently sized thermocouples and the steady-state nature of the profiles. The long-dashed straight lines were drawn from the measured throat temperature (Fig. 1) to the value measured at the deepest point in the liquid. No measurements could be made between these two points.

an unmoving water-vapor interface was present at the funnel mouth.

The temperature in each phase near the interface on the chamber center line was measured with a thermocouple (TC1) mounted on a rigid frame that was connected to a positioning micrometer. The position of the thermocouple was determined with the cathetometer. This thermocouple was small enough (25.4-μm diam) that its junction could be positioned in the liquid phase with little distortion of the interface. A second thermocouple (TC2, 81.3-μm diam) was also mounted on the frame. Its junction was 0.5 mm above that of the smaller junction. Both thermocouples were used to measure the temperature in the vapor phase. A third thermocouple was permanently positioned near the throat of the funnel. In the test-liquid reservoir, three thermocouples were present, positioned as indicated in Fig. 1. When the temperature profile, interface height, and (syringe) pumping rate were unchanging for 30 min, the system was judged to be in a steady state.

III. EXPERIMENTAL RESULTS

Once steady state had been reached, two temperature profiles in each phase were measured while the system was in steady state. The minimum steady-state periods for the evaporation and condensation experiments were 165 and 150 min, respectively. As indicated in Fig. 2, the temperatures measured with the differently sized thermocouples agreed to within $\pm 0.25\,^{\circ}\mathrm{C}$, indicating that any heat conduction along the thermocouple had little effect on the measurements. The positions closest to the interface in each phase where the temperatures were measured were 0.02 ± 0.01 mm above the interface, and 0.04 ± 0.01 mm below.

A. Temperature profiles in the liquid phase near the interface

The experiments were run in pairs. First, an evaporation experiment was conducted. The evaporation rate was chosen high enough so that the liquid interfacial temperature was less than $4\,^{\circ}\mathrm{C}$. The interface was the position of smallest temperature in the liquid phase. Since water expands on cooling for temperatures less than $4\,^{\circ}\mathrm{C}$, this ensured that during the evaporation experiments, the least dense liquid was at the interface, and no buoyancy-driven (or Rayleigh-Bénard) convection would be expected.

Then a corresponding condensation experiment was performed by approximately inverting the temperature profile in the liquid phase (see Table I and Fig. 2). This ensured that during the condensation experiments, the interfacial liquid temperature was above $4\,^{\circ}\mathrm{C}$ and was the highest temperature in the liquid phase. Thus, the least dense liquid was again at the interface. There was no buoyancy-driven convection in the vapor phase in either the evaporation or condensation experiments, since the lowest temperature was at the bottom of the vapor phase in each case. The temperature profiles in the liquid and vapor phases of experiments E1 and C1 (Tables I and II) are shown in Fig. 2.

If the imposed temperature profile does eliminate buoyancy-driven convection as these results suggest, surface-tension driven (or Marangoni-Bénard) convection is not necessarily eliminated. When the temperature profile in the liquid phase near the interface is closely examined, one finds a layer where the temperature is approximately uniform, and then deeper in the liquid phase the temperature has an approximately constant gradient. The uniform temperature layers of experiments E1 and C1 are easily seen in Figs. 3 and 4. For the evaporation experiments, the thickness of the uniform temperature layer varied from 0.35 to 0.61 mm and tended to decrease as the evaporation rate was increased. These thicknesses correspond to the highest and lowest evaporation fluxes, respectively.

For the condensation experiments, the uniform temperature layer ranged from 0.22 to 0.37 mm, but did not correlate with the condensation rate. The temperature profile near the interface measured for condensation experiment C4 is indicated in Fig. 5. The thickness of the uniform temperature layer in the liquid phase was 0.25 mm and the condensation flux was 0.04 g/s m^2. For experiment C1 (Fig. 4), the thickness of the uniform temperature layer was 0.22 mm and the condensation flux was 0.315 g/s m^2. Thus an order of magnitude change in the condensation flux did not significantly change the thickness of the uniform temperature layer.

B. Mode of energy transport in the liquid phase

The existence of an approximately uniform temperature layer near the interface but a constant gradient in temperature deeper in the liquid phase (see Figs. 3, 4, and 5) raises a question about the mode of energy transport in the liquid phase. This question is further complicated by the temperature discontinuity that was measured at the interface in each of the experiments. In evaporation experiment E1, the interfacial vapor temperature was measured 3 ± 1 mean-free paths (MFP's) above the interface and was greater than the

TABLE I. Measurements.

Expt. no.[a]	Liquid interface temp. T^L °C	Vapor interface temp. T^V °C	Temp. at throat TC3 °C	(z_0-z_f) Fig. 1 mm	Evaporation rate μg/s	Measured pressure in vapor phase Pa	Uniform temperature layer thickness, d mm
E1	−0.4± 0.05	2.6±0.05	26.1± 0.05	0.97	41.94 ±0.54	593±34	0.34
C1	25.6± 0.05	26.0± 0.05	0.00± 0.05	0.81	−12.73 ±0.12	3181 ±127	0.22
E2	−0.1± 0.05	2.8± 0.05	19.2± 0.05	0.95	41.82 ±0.31	639±34	0.38
C2	19.2± 0.05	19.5± 0.05	0.10± 0.05	1.37	−7.77 ±0.133	2161±86	0.37
E3	−0.2± 0.05	2.4± 0.05	12.5± 0.05	0.90	24.29 ±0.21	616±34	0.35
C3	12.6± 0.05	13.0± 0.05	0.00± 0.05	0.87	−6.088 ±0.16	1463±45	0.19
E4	−0.1± 0.10	2.5±0.10	7.10± 0.05	0.96	17.26± 0.2	629±34	0.61
C4	6.9± 0.06	7.5±0.06	−0.10± 0.05	1.06	−1.681 ±0.42	959±32	0.25

[a]The value of d_f in Fig. 1 was 7.0 mm in each experiment.

interfacial liquid temperature by 3.0±0.1 °C. When the direction of the net molecular transport at the interface was reversed by inverting the temperature profile in the liquid (experiment C1), the temperature discontinuity did *not* reverse. The interfacial vapor temperature, measured 8 ±3 MFP above the interface, was 0.4±0.1 °C greater than that in the liquid.

In all cases, evaporation or condensation, the interfacial temperature in the vapor was greater than that in the liquid. The magnitude of the temperature discontinuity increased with the evaporation flux, but a correlation between them could not be discerned for condensation, perhaps because the temperature in the vapor could only be measured several MFP's from the interface.

C. Measured pressure in the vapor phase

During the evaporation experiments, the chamber was continuously evacuated. The mean values of the vapor-phase pressure [±standard deviation (SD)] measured at the top of the chamber with the manometer (see Fig. 1) are listed in Table I. The error bars are the standard deviation calculated from measurements made during the steady-state period of each evaporation experiment.

During the condensation experiments, the chamber was closed, and the area of the liquid-vapor interface in the test-liquid reservoir was 24.5±1.3 times larger than that of the liquid-vapor interface at the top of the funnel. A separate set of control experiments was performed with a humidity sensor and mass spectrometer to determine if there would have been significant air leakage into the chamber during the con-

TABLE II. Predictions.

Expt. no.	Predicted vapor-phase pressure, P_{0e} Pa	Predicted liquid phase pressure on center line Pa	Interface radius on center line, R_0 mm	Evaporation flux g/m^2 s	Saturation pressure @T^V Pa	Saturation pressure @ T^L Pa
E1	592.4	617.3	6.088	1.017	766.6	593.0±2.2
C1	3282.0	3294.3	7.119	−0.315	3360.9	3281.9±9.9
E2	605.6	620.7	6.20	0.797	747.3	606.1±2.2
C2	2224.5	3300.7	4.545	−0.177	2266.4	2224.4±5.6
E3	601.3	615.8	6.506	0.595	726.2	601.7±2.2
C3	1458.8	3295.6	6.690	−0.150	1497.3	1458.7±4.5
E4	605.8	621.0	6.143	0.419	731.4	606.1±4.5
C4	994.81	3298.2	5.628	−0.040	1036.6	994.8±4.2

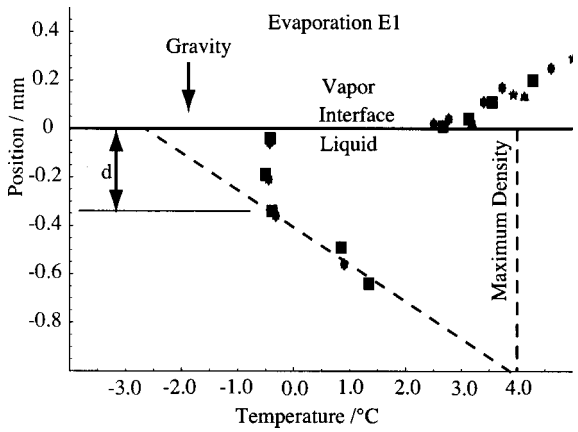

FIG. 3. Temperature measured near the interface on the vertical center line of the chamber during evaporation experiment E1. The experimental conditions are listed in Table I. Note the interfacial liquid temperature is below 4 °C, a temperature discontinuity was present at the interface in which the interfacial vapor temperature was greater than that in the liquid, immediately below the interface the temperature in the liquid phase was spatially uniform, and deeper in the liquid the temperature profile had a constant gradient.

densation experiments. These control experiments indicated the Hg manometer readings could have been slightly affected, but the vapor partial pressure corresponded closely to the saturation pressure of water based on the mean temperature of the test-liquid reservoir. This value is recorded in Table I for each condensation experiment.

D. Calculation of the interface shape

The Laplace equation was used to calculate the shape of the axisymmetric interface. If the pressure profile in each phase is assumed hydrostatic, this equation may be written in

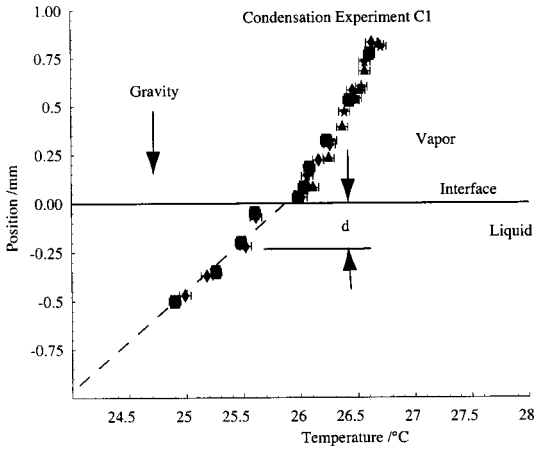

FIG. 4. Temperature measured near the interface on the vertical center line of the phase-change chamber during condensation experiment C1. Note the interfacial liquid temperature is above 4 °C, a temperature discontinuity was present at the interface in which the interfacial vapor temperature was greater than that in the liquid, the temperature immediately below the interface was spatially uniform, and deeper in the liquid the temperature profile had a constant gradient.

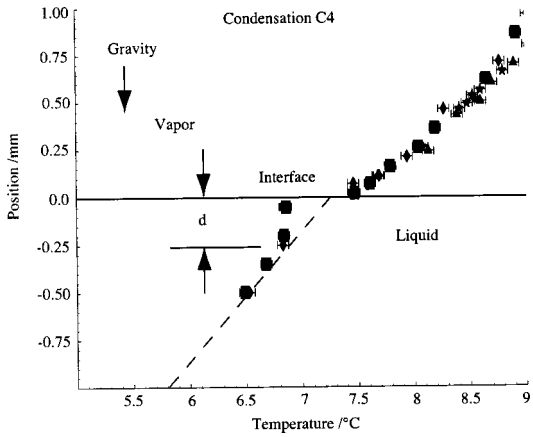

FIG. 5. Temperature measured near the interface on the vertical center line of the phase-change chamber during condensation experiment C4 (Table I). Note a temperature discontinuity was present at the interface in which the interfacial vapor temperature was greater than that in the liquid, the temperature immediately below the interface was spatially uniform, and deeper in the liquid the temperature profile had a constant gradient.

terms of the radial and axial positions on the interface, $r(\phi), z(\phi)$, and the turning angle ϕ (see Fig. 1):

$$\frac{dz}{d\phi} = \frac{-\sin\phi}{q}, \tag{1}$$

$$\frac{dr}{d\phi} = \frac{\cos\phi}{q}, \tag{2}$$

where

$$q = -\left(\frac{r(\phi)}{\sin\phi}\right) + W_g(z_0 - z)\left(\frac{1}{\nu^L_{\rm sat}(T^L)} - \frac{1}{\nu^V_{\rm sat}(T^V)}\right) + \frac{2}{R_0}, \tag{3}$$

and the molecular weight is denoted as W, the gravitational intensity as g, the radius of curvature on the center line as R_0, the specific volumes as $\nu^j_{\rm sat}$, and the temperature at the interface as T^j $(j=L,V)$. A superscript L or V indicates a property of the liquid or vapor phase and the subscript sat on a property that it is to be evaluated at the saturation condition.

The boundary conditions for the integration of these equations are provided by the values of the interface shape parameters, $z_0 - z_f$ and d_f. These parameters are defined in Fig. 1, and were measured in each experiment with the cathetometer. Their values are listed in Table I. This system of equations was solved numerically with R_0 and the maximum turning angle $\phi_{\rm Max}$ chosen to satisfy the conditions imposed by the measured values of the interface parameters.

The area of the interface may then be calculated from the function $r(\phi)$ that is obtained by this integration

$$A_{LV} = 2\pi \int_0^{\phi_{\rm Max}} \frac{r(\phi)}{q}\, d\phi. \tag{4}$$

The pressures in the liquid and vapor phases at the interface as a function of the turning angle are given by

$$P^L = P_0^V + \frac{2\gamma^{LV}}{R_0} + \frac{W_g}{\nu_{\text{sat}}^L}[z_0 - z(\phi)], \tag{5}$$

$$P^V = P_0^V + \frac{W_g}{\nu_{\text{sat}}^V}[z_0 - z(\phi)]. \tag{6}$$

Thus, the pressure at the interface in each phase may be calculated once the value of P_0^V has been determined. The interfacial pressure could not be measured directly, but it can be calculated and compared with that measured at the top of the chamber with the Hg manometer.

IV. INTERFACIAL CONDITIONS DURING PHASE CHANGE PROCESSES

The SRT expression for the net phase change rate is given in Appendix A. In summary, j_{LV} is in terms of the entropy change that results from one molecule making a transition from the liquid to the vapor phase, Δs_{LV} and the molecular exchange rate between the phases of an associated system K_e [23]. The associated system is defined by supposing that at one instant the steady-state system that we consider experimentally is isolated and allowed to evolve to equilibrium. When the isolated system has reached thermodynamic equilibrium, the molecular exchange rate between the liquid and vapor phases in the isolated system would be the value of K_e. The expression for j_{LV} [Eq. (A1) in the Appendix] is given by

$$j_{LV} = 2K_e \sinh(\Delta s_{LV}/k).$$

The expression for Δs_{LV} and K_e may be obtained from the closed, coupled system of equations, Eqs. (A1) through (A6). When the expressions for Δs_{LV} and K_e are inserted into Eq. (A1), it is found that the expression for j_{LV} is in terms molecular properties, material properties, and the interfacial, local equilibrium properties of each phase. The molecular properties include the molecular vibrational frequencies ω_l and the partition function for the molecule. The approximate expression given for the partition function in Eq. (A6) is for the triatomic water molecule. The material properties of the liquid and vapor phases that appear in the expression for j_{LV} are ν_{sat}^L, $P_{\text{sat}}(T)$, and γ^{LV}, and the local equilibrium properties of each phase are T^V, P^V, T^L, and R_0^{-1}. The center-line curvature R_0^{-1} could be replaced by the pressure P^L. The value of R_0 is determined from the measured interface parameters and the numerical integration of Eqs. (1)–(3).

A. Predicted pressure in the vapor phase

The total evaporation rate, J_{LV} may be obtained by integrating j_{LV} over the surface

$$J_{LV} = 2\pi \int_0^{\phi_{\text{Max}}} j_{LV} \frac{r(\phi)}{q} d\phi. \tag{7}$$

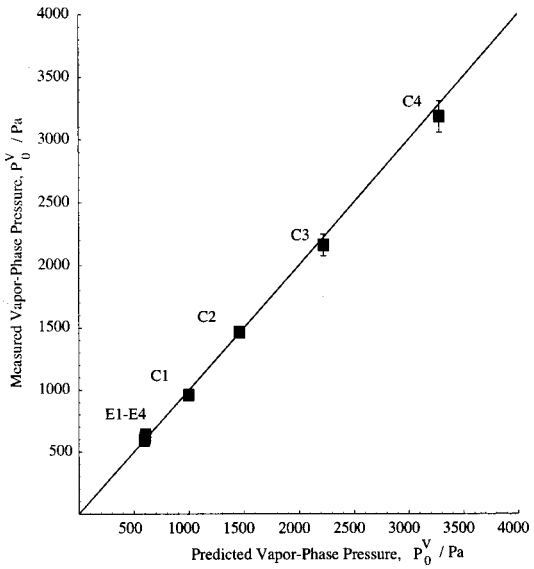

FIG. 6. Comparison of the predicted partial pressure of the vapor at the interface with that measured when either evaporation or condensation was occurring at the interface. Except in two cases, the error bars on the measured pressure are covered by the size of the symbols. The measured pressures are listed in Table I and the predicted values in Table II. Note that there is no measured disagreement between the measurements and the predictions.

When the measured values of T^L, T^V, R_0^{-1}, and J_{LV}, which are listed in Tables I and II, are used in Eqs. (1)–(7) and (A1)–(A6), a closed set of equations is obtained that contains the single unknown P_0^V. An iteration procedure may be used to calculate this vapor-phase pressure. The values determined by this procedure are listed in Table II. For each experiment, this predicted value of the vapor-phase pressure may be compared with the measured values. One finds the results shown in Fig. 6.

It has been previously found that SRT can be used to correctly predict the conditions at which evaporation of three different liquids including water takes place at a measured flux [21–23]. The results in Fig. 6 indicate that for water, SRT can be used equally well to predict the interfacial conditions when the direction of interfacial molecular flux is reversed so that condensation takes place.

Note from Table II that in each of the evaporation experiments, the predicted *vapor-phase* pressure, P_0^V is within a fraction of a pascal of the saturation pressure corresponding to the measured *liquid* interfacial temperature T^L. Compared to its own interfacial temperature T^V the vapor is predicted to be at a pressure less than $P_{\text{sat}}(T^V)$. Thus, the vapor phase is superheated. By contrast, the liquid phase is predicted to be at a pressure greater than $P_{\text{sat}}(T^L)$. Thus, the liquid phase is compressed.

When the direction of the net molecular flux is reversed, i.e., for the condensation experiments, these conditions are predicted *not* to reverse. In each condensation experiment, the predicted vapor-phase pressure is within 0.1 Pa of the saturation vapor pressure corresponding to the interfacial temperature of the *liquid*, $P_{\text{sat}}(T^L)$. The vapor phase remains superheated and the liquid compressed. However, compared

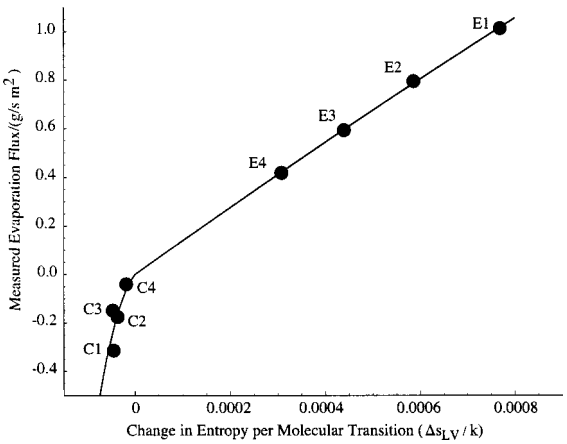

FIG. 7. Dependence of the evaporation flux on s_{LV}, the change in entropy that results when the one molecule is transferred from the liquid to the vapor phase. The prediction is that if s_{LV} is negative, the evaporative flux will also be negative (condensation).

to the conditions for evaporation, the degree of vapor superheating is reduced and the degree of liquid phase compression is increased.

B. The potential for molecular transport at an interface

We note that in classical kinetic theory, the assumption is usually made that the liquid evaporates at a rate determined only by the conditions existing in that phase [1–3]. However, SRT indicates the conditions in each phase play a role in determining the net flux rate. For example [23], the unidirectional evaporation flux r_{LV} is given by

$$r_{LV}=K_e \exp\left[\frac{s_{LV}}{k}\right], \tag{8}$$

and the unidirectional condensation flux by

$$r_{VL}=K_e \exp\left[\frac{-s_{LV}}{k}\right]. \tag{9}$$

(The net evaporation flux, j_{LV} is the difference between r_{LV} and r_{VL}.) As indicated in Eq. (A2), s_{LV} depends on the chemical potentials and temperatures in the liquid and the vapor phases. Thus, unlike classical kinetic theory, the unidirectional rate of evaporation or the unidirectional condensation rate depends on the conditions in each phase.

If Eq. (A1) is examined, it is found that evaporation is predicted to occur when Δs_{LV} is positive, and condensation is predicted to result when Δs_{LV} is negative. Since P_0^V has been calculated for each experiment, this prediction may be examined. The value of the pressure in each phase at any position on the liquid-vapor interface may be calculated using Eqs. (5) and (6). Then assuming the interfacial temperature in each phase to be approximately equal to the values measured on the center line, the values of Δs_{LV} at the interface may be calculated from Eq. (5). There is only a small variation in the value of Δs_{LV} with position on the interface. In all of the experiments, the maximum variation was $\sim 10^{-3}\%$. Thus, the mean value of Δs_{LV} may be used to calculate the evaporation flux in each experiment. One finds the results indicated in Fig. 7.

As seen there, the measured values of j_{LV} are negative (condensation) when Δs_{LV} is negative, and j_{LV} is positive when Δs_{LV} is positive (evaporation). Thus, Δs_{LV} acts as a potential to determine the direction of molecular transport in a fashion similar to the way temperature acts to determine the direction of thermal energy transport.

C. The temperature profile during the liquid-vapor phase transition

When either evaporation or condensation is taking place, the measured temperature profiles indicate: (1) A temperature discontinuity exists at the liquid-vapor interface, and independently of the phase change direction, the temperature is always greater in the vapor. The magnitude of the temperature discontinuity increases with the evaporation flux. During condensation, the temperature could only be measured $\sim$10 MFP's from the interface, and a relation between it and the condensation flux could not be discerned from measurements made at this distance from the interface. (2) In the liquid phase immediately below the surface, the temperature is approximately spatially uniform for a depth that depends on the phase change process, but is on the order of $\sim$0.5 mm. (3) Below the uniform temperature layer, the temperature profile in the liquid was observed to have a constant gradient, indicating the mode of energy transport there is thermal conduction.

The existence of the uniform temperature layer and the constant temperature gradient in the subinterface region suggests that surface-tension driven convection is present in the liquid near the interface. A complete description of the energy transport must explain the temperature discontinuity.

We note that when equilibrium exists between the liquid and vapor phases of water, the temperature would be the same in each phase, but the average energy per molecule would be $\sim$2 orders of magnitude higher in the vapor than in the liquid. The fact that during evaporation the measured interfacial vapor temperature is higher than in the liquid suggests that it is predominantly the molecules from the high-energy tail of the energy distribution that are able to escape the liquid. This suggestion is supported by previous studies of the steady-state evaporation of water, octane or methylcyclohexane [21–23]. For each substance, the interfacial vapor temperatures were measured to be greater than that in the liquid. The magnitude of the temperature discontinuity varied from one substance to another, but for each substance it increased as the evaporation rate was increased. At the highest evaporation rate of water, the temperature in the vapor was measured within approximately one MFP of the interface and was 7.8°C higher than that on the liquid side of the interface. Thus, on average the molecules encountered the thermocouple simultaneously with their first collision. It appears the higher-energy molecules were coming right out of the liquid.

We note that the explanation in terms of the energy distribution is based on single-particle events. Bedeaux and

Kjelstrup [24] have suggested that multiple particle events are necessary to explain the observed temperature discontinuities reported by Fang and Ward [21,22]. Also, it has been pointed out by Fang and Ward [21–23] that if it is assumed that the evaporation and condensation coefficients are equal to unity, classical kinetic theory leads to a prediction of a temperature discontinuity for evaporation in the opposite direction from that measured; however, for condensation, the predicted temperature discontinuity is in the same direction as that predicted from classical kinetic theory on this basis, but much smaller than that measured [25–28].

A much larger temperature discontinuity (''a few million degrees'') has been thought to exist at the solar corona-photospheric chormospheric ''surface'' for some time [29] and recent results confirm its existence [30]. Although the solar circumstance is much more complex than the one we consider, there are conceptual similarities. If one thinks of the solar surface heating the corona, it would be impossible for the corona to be hotter than the surface, but if one thinks of the higher-energy particles escaping the surface, there is no reason the corona could not have a higher temperature. Similarly, if during evaporation, the molecules of higher energy are the ones escaping the liquid, there is no reason the interfacial vapor temperature could not be higher than that of the liquid.

For fluid evaporation, an estimate of the molecular energy of the escaping molecules above the average would be $T^L \Delta s_{LV}$. Note that under equilibrium conditions Δs_{LV} is zero and that as the evaporation flux increases, Δs_{LV} increases, as does the temperature discontinuity. The depletion of the interface layer of the higher-energy molecules by this ''energy-partitioning'' would give rise to an equilibration or mixing process that could contribute to the molecules in the layer near the surface having a uniform temperature.

The predicted necessary condition for condensation is that Δs_{LV} is negative. A negative value of Δs_{LV} indicates there is an increase in entropy when a molecule transfers from the vapor to the liquid. Molecular transfers in both directions are predicted, but a larger number is predicted to transfer in the direction of increasing entropy than in the reverse direction. The fact that the temperature is higher in the vapor than in the liquid during steady-state condensation indicates that there is a preferential transfer of the lower energy molecules from the superheated vapor to the compressed liquid phase. A measure of the energy of the molecules transferring from the vapor to the liquid would be $T^V \Delta s_{LV}$. The equilibration of these molecules with the others in the liquid phase would also give rise to a mixing process.

Thus, there are at least two processes that could contribute to establishing a uniform temperature in the liquid near the interface—surface-tension driven convection and ''energy partitioning'' during the phase change process. Since there is no criterion available to determine when surface-tension driven convection can be expected that can be applied for the experimental circumstances we consider, the conclusion that surface-tension driven convection is in part responsible for the uniform temperature layer must be viewed as tentative.

V. CONCLUSION

In both the evaporation and condensation experiments the measured temperature profile indicates thermal conduction in a subinterface liquid region, a uniform temperature layer ($\sim$0.5 mm) in the liquid near the interface, and a temperature discontinuity at the interface in which the interfacial vapor temperature is greater than that of the liquid. Although the experimental conditions are such that there is no buoyancy-driven convection, the uniform-temperature layer suggests a ''mixing'' process in the liquid phase near the interface. One possible source of the mixing is surface-tension driven convection. Another is the ''energy partitioning'' at the interface that is required to account for the measured temperature discontinuity.

The SRT approach gives the expression for the phase change flux j_{LV} in terms of molecular and material properties of the substance undergoing the phase change process, and the interfacial, local equilibrium properties in each phase, T^L, T^V, R_0^{-1}, and P^V. The molecular and material properties for water are known; thus by measuring the phase change flux and three of the four local equilibrium properties, an unequivocal prediction can be made of the fourth. This procedure has been used to predict the vapor-phase pressure. For each experiment, the measured interfacial temperatures, interface curvature and phase change rate were used in the SRT expression and the vapor-phase pressure, P^V predicted. The predictions indicate that during the phase change process, the pressure in the *vapor* is very near the saturation vapor pressure corresponding to the interfacial *liquid* temperature $P_{\text{sat}}(T^L)$, and when the predicted values of P^V are compared with the measured vapor-phase pressures, very close agreement is found for both evaporation and condensation.

One of the significant differences between the SRT expression for the net phase change rate and that of classical kinetic theory is that SRT indicates the unidirectional rate of evaporation r_{LV} is affected not only by the state of the liquid, but also by the state of the vapor. Similarly, the unidirectional rate of condensation r_{VL} is predicted to depend on the thermodynamic state of each phase. The net rate (i.e., $r_{LV} - r_{VL}$) is predicted to be in terms of change in entropy that results from one molecule transferring from the liquid to the vapor phase s_{LV}. When s_{LV} is positive, the net rate is predicted to be evaporation, and if s_{LV} is negative the rate is predicted to be condensation. But the value of s_{LV} depends on the thermodynamic properties in each phase, see Eq. (A2).

As a result of this dependence, during steady-state evaporation, it is predicted that the liquid is at a pressure greater than $P_{\text{sat}}(T^L)$ and the vapor is at a pressure less than $P_{\text{sat}}(T^V)$; thus the liquid is compressed and the vapor is superheated. When the net molecular flux at the interface is reversed to produce steady-state condensation, it is found that the degree to which the liquid is compressed is increased and the degree to which the vapor is superheated is reduced.

ACKNOWLEDGMENT

This study was supported by the Canadian Space Agency and the Natural Sciences and Engineering Research Council of Canada.

APPENDIX

The expression for the net evaporative flux j_{LV} that is obtained from SRT is in terms of two thermodynamic functions, Δs_{LV} and K_e and may be written [23]

$$j_{LV}=2K_e \sinh(\Delta s_{LV}/k), \tag{A1}$$

where k is the Boltzmann constant. Local equilibrium is assumed valid in each phase, and if the chemical potential at the interface in phase i is denoted as $\boldsymbol{\mu}^i$ and the temperature by T^i, then the function s_{LV} may be written

$$\Delta s_{LV}=\left(\frac{\mu^L}{T^L}-\frac{\mu^V}{T^V}\right)+h^V\left(\frac{1}{T^V}-\frac{1}{T^L}\right), \tag{A2}$$

where h^V is the intensive enthalpy in the vapor phase. The thermodynamic function K_e may be expressed

$$K_e=\frac{P_{\rm sat}(T^L)\exp\left(\dfrac{v^L_{\rm sat}}{kT^L}[P^L_{0_e}-P_{\rm sat}(T^L)]\right)}{\sqrt{2\pi mkT^L}}, \tag{A3}$$

where the pressure $P^L_{0_e}$ is determined as the iterative solution of

$$P^L_{0e}=P_{\rm sat}(T^L)\exp\left[\frac{v^L_{\rm sat}}{kT^L}[P^L_{0e}-P_{\rm sat}(T^L)]\right]+\frac{2\gamma^{LV}(T^L)}{R_0}. \tag{A4}$$

An approximate expression for Δs_{LV} has been given [23],

$$\begin{aligned}\frac{\Delta s_{LV}}{k}=&4\left(1-\frac{T^V}{T^L}\right)+\left(\frac{1}{T^V}-\frac{1}{T^L}\right)\sum_{l=1}^{3}\left(\frac{\hbar\omega_l}{2k}\right.\\&\left.+\frac{\hbar\omega_l/k}{\exp(\hbar\omega_l/kT^V)-1}\right)+\frac{v^L_{\rm sat}}{kT^L}[P^L-P_{\rm sat}(T^L)]\\&+\ln\left[\left(\frac{T^V}{T^L}\right)^4\left(\frac{P_{\rm sat}(T^L)}{P^V}\right)\right]+\ln\left(\frac{q_{\rm vib}(T^V)}{q_{\rm vib}(T^L)}\right),\end{aligned} \tag{A5}$$

where $q_{\rm vib}$ is the vibrational partition function:

$$q_{\rm vib}=\prod_{l=1}^{3}\frac{\exp[-\hbar\omega_l/(2kT)]}{1-\exp(-\hbar\omega_l/kT)}. \tag{A6}$$

For the water molecule, the three measured vibrational frequencies [31] have values of 1590, 3651, and 3756 $\rm cm^{-1}$.

[1] H. Hertz, Ann. Phys. (Leipzig) **17**, 177 (1882).
[2] J. Stefan, Weiner Ber. **68**, 385 (1873); **98**, 1418 (1889).
[3] M. Knudsen, Ann. Phys. (Leipzig) **28**, 75 (1908).
[4] O. Knacke and I. N. Stranski, Prog. Met. Phys. **6**, 181 (1956).
[5] R. Marek and J. Straub, Int. J. Heat Mass Transf. **44**, 39 (2001).
[6] A-T. Chai and N. Zhang, Exp. Heat Transfer **11**, 187 (1998).
[7] M. Assenheimer and V. Steinberg, Phys. Rev. Lett. **70**, 3888 (1993).
[8] H. K. Cammenga, D. Schreiber, G. T. Barnes, and D. S. Hunter, J. Colloid Interface Sci. **98**, 585 (1984).
[9] G. T. Barnes and D. S. Hunter, J. Colloid Interface Sci. **88**, 437 (1982).
[10] H. K. Cammenga, D. Schreiber, and B.-E. Rudolph, J. Colloid Interface Sci. **92**, 181 (1983).
[11] D. Schreiber and H. K. Cammenga, Ber. Bunsenges. Phys. Chem. **85**, 909 (1981).
[12] J. R. A. Pearson, J. Fluid Mech. **4**, 489 (1958).
[13] D. A. Nield, J. Fluid Mech. **19**, 341 (1964).
[14] A. Ye. Rednikov, P. Colinet, M. G. Velarde, and J. C. Legros, J. Fluid Mech. **405**, 57 (2000).
[15] C. A. Ward, R. D. Findlay, and M. Rizk, J. Chem. Phys. **76**, 5599 (1982).
[16] C. A. Ward, J. Chem. Phys. **79**, 5605 (1983).
[17] M. Torri and J. A. W. Elliott, J. Chem. Phys. **111**, 1686 (1999).
[18] J. A. W. Elliott and C. A. Ward, J. Chem. Phys. **106**, 5677 (1997).
[19] J. A. W. Elliott, H. Y. Elmoazzen, and L. E. McGann, J. Chem. Phys. **113**, 6573 (2000).
[20] J. A. W. Elliott and C. A. Ward, J. Chem. Phys. **106**, 5667 (1997).
[21] G. Fang and C. A. Ward, Phys. Rev. E **59**, 417 (1999).
[22] G. Fang and C. A. Ward, Phys. Rev. E **59**, 441 (1999).
[23] C. A. Ward and G. Fang, Phys. Rev. E **59**, 429 (1999).
[24] D. Bedeaux and S. Kjelstrup, Physica A **270**, 413 (1999).
[25] Y.-P. Pao, Phys. Fluids **14**, 1340 (1971).
[26] Y. Sone and Y. Onishi, J. Phys. Soc. Jpn. **35**, 1773 (1973).
[27] J. W. Cipolla Jr., H. Lang, and S. K. Loyalka, J. Chem. Phys. **61**, 69 (1974).
[28] K. Aoki and C. Cercignani, Phys. Fluids **26**, 1163 (1983).
[29] J. D. Scudder, Astrophys. J. **398**, 319 (1992).
[30] M. J. Aschwanden, R. W. Nightingale, and D. Alexander, Astrophys. J. **541**, 1059 (2000).
[31] G. Herzberg, *Molecular Spectra and Molecular Structure* (Van Nostrand, Princeton, NJ, 1964), Vol. 2, p. 281.